

# Coupling immersed boundary-lattice Boltzmann method with smoothed point interpolation method for large-displacement fluid-structure interaction problems

\*S.Q. Wang<sup>1</sup>, Y.N. Cai<sup>1</sup>, †G.Y. Zhang<sup>1,2,3</sup>, S. Li<sup>1,2,3</sup>, and J.H. Lu<sup>1,3</sup>

<sup>1</sup>Liaoning Engineering Laboratory for Deep-Sea Floating Structures, School of Naval Architecture, Dalian University of Technology, Dalian, 116024, P. R. China

<sup>2</sup>State Key Laboratory of Structural Analysis for Industrial Equipment, Dalian University of Technology, Dalian, 116024, P. R. China

<sup>3</sup>Collaborative Innovation Center for Advanced Ship and Deep-Sea Exploration, Shanghai, 200240, P. R. China

\*Presenting author: wangsqyzx@163.com

†Corresponding author: gyzhang@dlut.edu.cn

## Abstract

The immersed boundary-lattice Boltzmann method (IB-LBM) has been verified to be an effective tool for fluid-structure interaction (FSI) simulation associated with thin and flexible body, and the newly developed smoothed point interpolation method (S-PIM) can handle the largely deformable solids owing to its soften model stiffness of model and insensitivity to mesh distortion. In this work, a novel method has been proposed in the present work by coupling IB-LBM with S-PIM for FSI problems with large-displacement solids. The proposed method preserves the efficiency of LBM for fluid solver, utilizes S-PIM to establish the realistic constitutive laws for nonlinear solids, and avoids the mesh regeneration based on the frame of immersed boundary method (IBM). Three benchmarking examples have been carried out to validate the accuracy, convergence and stability of the proposed method in consideration of comparative results with referenced solutions.

**Keywords:** immersed boundary-lattice Boltzmann method; smoothed point interpolation method; fluid-structure interaction (FSI); constitutive laws

## Introduction

Fluid-structure interaction problems (FSI) are common in many fields in light of two-phase interaction when the movement or distortion of the body arises due to the external force exerted by the neighboring fluid and the corresponding response also has an impact on the fluid domain. The complicated mechanism requires an efficient and reliable tool especially for largely deformable nonlinear solids/structures. The immersed boundary method (IBM) has been successfully applied in the simulation of interaction between the fluid and the moving interface, and the mesh regeneration can be avoided using non-boundary-fitted grid [1]. It assumes the fluid around the interface is affected by a kind of body force which allows the solver of Navier-Stokes equations based on the fixed Euler grid, and the configuration together with shape of the boundary would not be taken into consideration. Hence, the solver process for FSI problems has been simplified in comparison with the boundary-fitted grid

method.

Generally, one can use the finite element method (FEM) or finite volume method (FVM) to handle the Navier-Stokes equations in FSI simulation. However, the solver for the nonlinear convection term may bring about the nonphysical numerical oscillation and the special format of FEM or FVM need be constructed such as pressure-stabilized Petrov-Galerkin (PSPG) formulation [2] and characteristic-based split (CBS) algorithm [3] which may consume additional calculation resource. And the pressure Poisson equation should be considered for the incompressible viscous flow based on these traditional methods which also affect the calculation efficiency. Then the lattice Boltzmann method (LBM) was introduced and has been widely used in the CFD field during the past two decades. Based on the explicit algorithm, LBM can avoid the shortcoming of FEM and FVM and guarantee the accuracy and efficiency with the simple form as well as easy operation. And the immersed boundary-lattice Boltzmann method (IB-LBM) was proposed for FSI simulation in consideration of the same discretization using Cartesian mesh in IBM and LBM [4]. The further development and improvement have been achieved for various FSI problems [5-7].

FEM is a popular solver for the transient analysis of nonlinear solids and structures. And the simple triangular element with three nodes (T3) for 2D or tetrahedron element with four nodes (T4) for 3D are very suitable for the preprocessing especially encountered with complex domain. However, some disadvantages have limited the extensive application like the overly-stiff performance and the poor accuracy. Then a class of gradient/stain smoothing methods have been proposed to improve the performance of T3/T4 cells including smoothed finite element methods (S-FEM) [8, 9] and smoothed point interpolation methods (S-PIM) [10, 11]. Compared to S-FEM, S-PIM allows the discontinuous displacement function in the smoothed domain by constructing a weakened-weak form in  $G$  space. Based on different smoothed domains, ES-PIM and NS-PIM can be constructed and used for linear and nonlinear analysis.

IB-LBM has been verified as an efficient tool for FSI simulation and S-PIM also can handle the complex nonlinear constitutive equation well. Coupling IB-LBM with S-PIM, this article puts forward a novel method for FSI problems involved with the large deformable nonlinear solids and structures. And Figure 1 has shown the general procedure. The fluid and solid can be separated from the FSI system, and solved based on fixed Euler grids by LBM and moving Lagrange grids by S-PIM. The coupling force has been calculated by the frame of IBM and the information exchange can be implemented by the interpolation of the delta function.

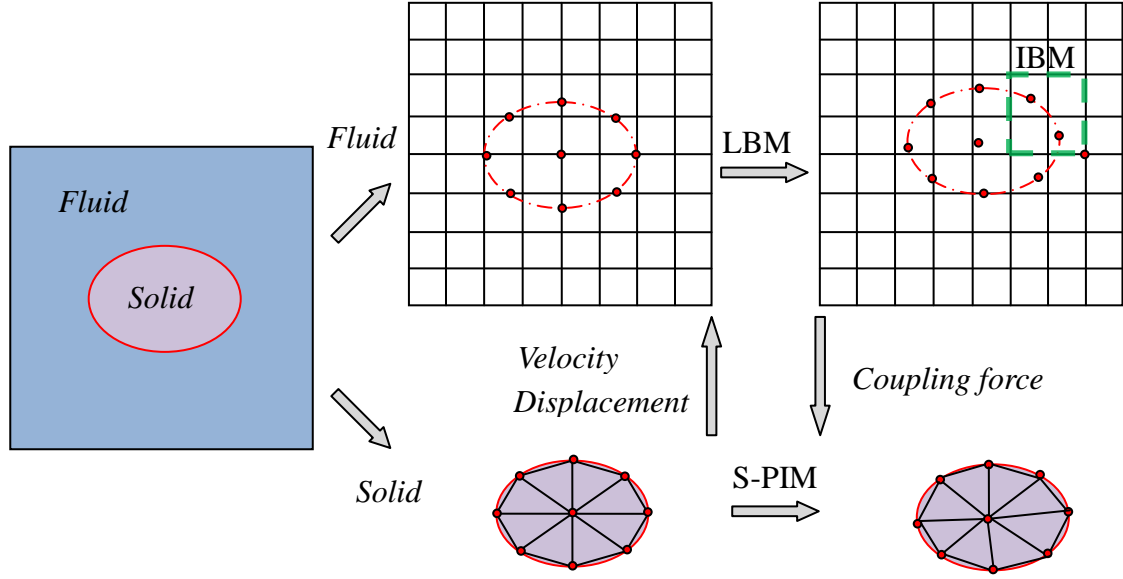


**Figure 1** The general procedure of coupling S-PIM with IB-LBM

### Immersed boundary-lattice Boltzmann method (IB-LBM)

For the incompressible fluid flows, the evolution equation of LBE [12] can be written as:

$$f_{\alpha}(\mathbf{x} + \mathbf{c}_{\alpha}\delta t, t + \delta t) - f_{\alpha}(\mathbf{x}, t) = -\frac{f_{\alpha}(\mathbf{x}, t) - f_{\alpha}^{eq}(\mathbf{x}, t)}{\tau} + F_{\alpha}\delta t \quad (1)$$

where  $\mathbf{x}$  is the lattice coordinate,  $\mathbf{c}_{\alpha}$  are the velocities of particles,  $f_{\alpha}$  is the distribution function of particles,  $f_{\alpha}^{eq}$  is the corresponding equilibrium distribution,  $\tau$  is the relaxation time, and  $F_{\alpha}$  is the discrete force distribution function.

The particle velocity  $\mathbf{c}_{\alpha}$  is defined as follows using D2Q9 model [13]:

$$\mathbf{c}_{\alpha} = \begin{cases} (0, 0), & \alpha = 0, \\ (\cos[(\alpha - 1)\pi / 2], \sin[(\alpha - 1)\pi / 2]c, & \alpha = 1, 2, 3, 4, \\ (\cos[(\alpha - 1)\pi / 2], \sin[(\alpha - 1)\pi / 2]c, & \alpha = 5, 6, 7, 8. \end{cases} \quad (2)$$

where the velocity  $c = \delta x / \delta t$ .

The equilibrium distribution function  $f_{\alpha}^{eq}$  can be written in the following form:

$$f_{\alpha}^{eq} = \rho w_{\alpha} \left[ 1 + \frac{\mathbf{c}_{\alpha} \cdot \mathbf{u}}{c_s^2} + \frac{(\mathbf{c}_{\alpha} \cdot \mathbf{u})^2}{2c_s^4} - \frac{\mathbf{u}^2}{2c_s^2} \right] \quad (3)$$

where the sound velocity  $c_s = c / \sqrt{3}$ , and the factor  $w_{\alpha}$  is selected as  $w_0 = 0, w_{1-4} = 1/9$  and  $w_{5-8} = 1/36$ .

The discrete force distribution function  $F_{\alpha}$  can be expressed as follows:

$$F_\alpha = (1 - \frac{1}{2\tau})\omega_\alpha [\frac{\mathbf{c}_\alpha - \mathbf{u}}{c_s^2} + \frac{\mathbf{c}_\alpha \cdot \mathbf{u}}{c_s^4} \mathbf{c}_\alpha] \cdot \mathbf{f} \quad (4)$$

where  $\mathbf{f}$  is the external force.

By means of the mesoscopic model, the macroscopic variables like density and velocity can be obtained as:

$$\rho = \sum_{\alpha=0}^8 f_\alpha \quad (5)$$

$$\rho \mathbf{u} = \sum_{\alpha=0}^8 c_\alpha f_\alpha + \frac{1}{2} \mathbf{f} \delta t \quad (6)$$

The kinematic viscosity  $\nu$  is determined by:

$$\nu = c_s^2 (\tau - \frac{1}{2}) \delta t \quad (7)$$

There are several measures to evaluate the boundary force, and the present work adopts the direct forcing technique which was illustrated in Kang's paper [14]. The boundary force density at the  $m$ th Lagrangian point  $\mathbf{X}_m$  can be obtained as follows:

$$\mathbf{F}(\mathbf{X}_m, t) = 2\rho(\mathbf{U}^d(\mathbf{X}_m, t) - \mathbf{U}^*(\mathbf{X}_m, t)) / \delta t \quad (8)$$

where  $\mathbf{U}^d$  is the solid boundary velocity, and  $\mathbf{U}^*$  is the evolution velocity of fluid in Lagrangian mesh without force modification which can be interpolated from the neighboring Eulerian points:

$$\mathbf{U}^*(\mathbf{X}_m, t) = \sum_{(i,j)} \mathbf{u}^*(\mathbf{x}_{ij}, t) \delta_h(\mathbf{x}_{ij} - \mathbf{X}_m) h^2 \quad (9)$$

where  $\mathbf{x}_{ij}$  is the Euler node coordinate,  $\delta_h$  is a continuous kernel distribution to approximate the delta function, and  $h$  is the mesh size.  $\mathbf{u}^*$  is the evolution velocity in Eulerian points and evaluated with the following formula:

$$\rho \mathbf{u}^* = \sum_{\alpha=0}^8 c_\alpha f_\alpha \quad (10)$$

Once the boundary force density of the Lagrangian points is given, it can be distributed into the Eulerian points around it:

$$\mathbf{f}(\mathbf{x}_{ij}, t) = \sum_{b=0}^N \mathbf{F}(\mathbf{X}_b, t) \delta_h(\mathbf{x}_{ij} - \mathbf{X}_b) h \Delta s \quad (11)$$

where  $N$  is the total number of boundary nodes and  $\Delta s$  is the distance of adjacent Lagrangian points. And the boundary force density  $\mathbf{F}(\mathbf{X}_m, t)$  can be used to calculate the FSI force exerted on the solid by the boundary integrals.

### Smoothed point interpolation method (S-PIM)

If a group of  $N_n^s$  nodes and  $N_{ele}^s$  triangular background cells are used to discretize the solid domain  ${}^0\Omega^s$ . The displacement  $u_i^s$ , velocity  $v_i^s$  and acceleration  $a_i^s$  can be interpolated by the proper shape function  ${}^0\Phi_I^s$ :

$$u_i^s = \sum_I {}^0\Phi_I^s u_{ii}^s, v_i^s = \sum_I {}^0\Phi_I^s v_{ii}^s, a_i^s = \sum_I {}^0\Phi_I^s a_{ii}^s \quad (12)$$

where  ${}^0\Phi_I^s$  is the FEM shape function calculated at the initial configuration.

The gradient/strain smoothing technique is introduced in S-PIM based on the smoothed domain to soften the model stiffness, which is the main difference from the FEM. Suppose the domain  ${}^0\Omega^s$  is divided into  $N_{sd}^s$  smoothing domain  ${}^0\Omega_{isd}^{sd}$  with boundaries  ${}^0\Gamma_{isd}^{sd}$  ( $isd=1,2,\dots, N_{sd}^s$ ). Each smoothing domain  ${}^0\Omega_{isd}^{sd}$  is non-overlapped and covers the total calculation together. The smoothed displacement gradient in  ${}^0\Omega_{isd}^{sd}$  can be achieved using the displacement gradient  $u_{i,j}^s$  in the following form [15]:

$$\bar{u}_{i,j}^s(x_L) = \sum_I \left( \frac{1}{A_{isd}^{sd}} \int_{{}^0\Gamma_{isd}^{sd}} {}^0\Phi_I^s(x^s) n_j^{sd} d\Gamma \right) u_{ii}^s = \sum_I \frac{1}{A_{isd}^{sd}} \sum_n W_n \left( {}^0\Phi_I^s(x^s) n_j^{sd} \right) u_{ii}^s \quad (13)$$

where,  $\bar{u}_{i,j}^s(x_L)$  is the smoothed displacement gradient,  $A_{isd}^{sd}$  is the area of the smoothing domain,  $n_j^{sd}$  is the outward surface normal of the smoothing domain boundary  ${}^0\Gamma_{isd}^{sd}$ ,  $I$  is the number of nodes in smoothing domain,  $n$  is the number of gauss points, and  $W_n$  is the weight coefficient.

In the nonlinear analysis of solids, the deformation gradient,  $F_{ij} = u_{i,j} + \delta_{ij}$ , is the primary strain measure. The smoothing operation on the deformation gradient  $F_{ij}$  yields the following smoothed deformation gradient  $\bar{F}_{ij}^s$ :

$$\bar{F}_{ij}^s(X_{isd}^s) = \frac{1}{A_{isd}^{sd}} \int_{{}^0\Gamma_{isd}^{sd}} {}^0\Phi_I^s(X^s) n_j^{sd} d\Gamma u_{ii}^s + \delta_{ij} \quad (14)$$

Then other smoothed variables can be obtained such as the smoothed Green strain and the smoothed second Piola-Kirchhoff (PK2) stress using the smoothed deformation gradient.

The transient solutions of the nonlinear solids are achieved using the well-developed explicit time integration based on the central difference algorithm. The discretized equation of motion is given in the following form:

$$M_{IJ}^s a_{ji}^s = f_{ii}^{s,ext} - f_{ii}^{s,int} \quad (15)$$

where  $M_{IJ}^s$  is the lumped mass matrix,  $f_{ii}^{s,int}$  is the internal force vector defined in the total Lagrangian formulation, and  $f_{ii}^{s,ext}$  is the external force vector in the standard FEM form:

$$f_{ii}^{s,int} = \int_{\Omega^s} \Phi_{I,j}^s P_{ji}^s d\Omega \quad (16)$$

$$f_{ii}^{s,ext} = \int_{\Omega^s} \Phi_J^s \rho^s g_i d\Omega + \int_{\Gamma^s} \Phi_J^s \bar{T}_i d\Gamma \quad (17)$$

Considering the solid immersed in the fluid domain, we can get:

$$\int_{\Gamma^s} \Phi_J^s \bar{T}_i d\Gamma = f_i^{s,FSI} \quad (18)$$

where  $f_i^{s,FSI}$  denotes the FSI force.

## Numerical examples

### *Lid-driven cavity flow with a soft wall*

In this example, a lid-driven cavity flow with a hyperelastic wall is analyzed which can be considered a benchmark FSI problem and has been verified by some previous algorithms including ALE [16], IFEM [17] and IS-FEM [15]. As is illustrated in Figure 2(a), the size of the square cavity is  $L=2$  cm and the soft wall is located at the bottom with the length  $L=2$  cm and the height  $H=0.5$  cm. The fluid properties are given as the density  $\rho^f = 1.0$  g/cm<sup>3</sup> and the viscosity  $\mu^f = 0.2$  g/(cm·s). A simplified Mooney-Rivlin material is used to model the hyperelastic wall with the material constants  $C_{10} = 0.1$  g/(cm·s<sup>2</sup>),  $C_{01} = 0$  and  $\kappa = 0$  and the density is set as  $\rho^s = 1.0$  g/cm<sup>3</sup>. The top lid is driven by the following velocity distribution:

$$v_1^f = 0.5 \begin{cases} \sin^2(\pi x / 0.6) & x_1^f \in [0.0, 0.3] \\ 1.0 & x_1^f \in (0.3, 1.7) \\ \sin^2(\pi(x-2.0) / 0.6) & x_1^f \in [1.7, 2.0] \end{cases} \quad (19)$$

The other boundaries of the fluid domain satisfy the non-slip boundary condition, and the pressure at the midpoint of the bottom edge is set as zero to be a reference value. The top edge of the solid is free while the others are fixed. The fluid domain is divided into 200×200 uniform grids and the solid wall is discretized by irregular triangle elements with 976 nodes. Figure 2(b) shows the result of fluid velocity contour and the configuration of elastic wall, which is consistent with the previous study.

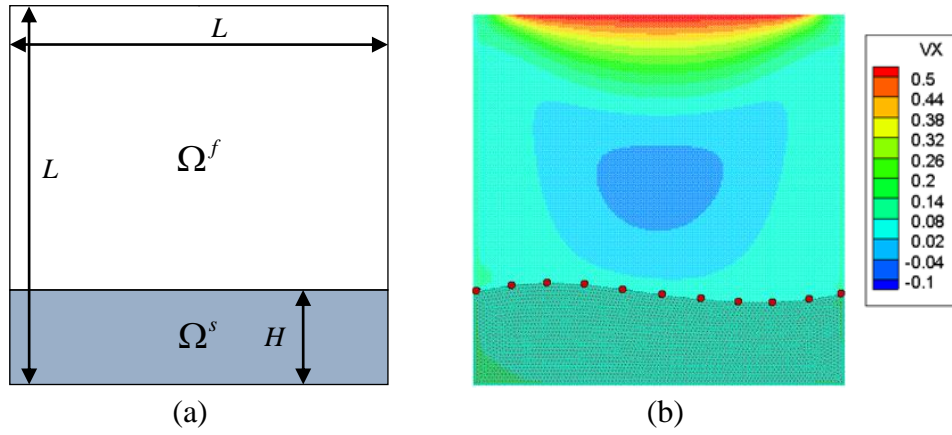


**Figure 2 A elastic wall in a lid-driven cavity flow (a) initial setting (b) Simulation result and the red circle denotes the result obtained by Ref [16]**

Then the analysis of convergence and stability would be carried out for the present method by a group of meshes setting. For the test of the fluid, the grid sizes of fluid domain are set as  $h^f=0.1, 0.08, 0.05, 0.04,$  and  $0.02$ , which are corresponding to the same solid element size of  $h^s=0.02$ . The reference solution is obtained using  $h^f=0.01$  and  $h^s=0.02$ . And for the test of solid, the grid sizes of solid domain are set as  $h^s=0.04, 0.036, 0.032, 0.028,$  and  $0.024$ , which are corresponding to the same fluid element size of  $h^f=0.04$ . The reference solution is obtained using  $h^f=0.04$  and  $h^s=0.02$ . We calculate the  $L^2$  norms of errors in the fluid velocity and solid displacement via the following formulas:

$$e_v^f = \frac{\|v_i^{f,num} - v_i^{f,ref}\|_{L_2}}{\|v_i^{f,ref}\|_{L_2}}, e_u^s = \frac{\|u_i^{s,num} - u_i^{s,ref}\|_{L_2}}{\|u_i^{s,ref}\|_{L_2}} \quad (20)$$

where  $v_i^{f,num}$  and  $u_i^{s,num}$  are the numerical solutions, and  $v_i^{f,ref}$  and  $u_i^{s,ref}$  are the reference solutions respectively. And the result can be seen in Figure 3 and 4 which verifies the good convergence and stability of the proposed method.

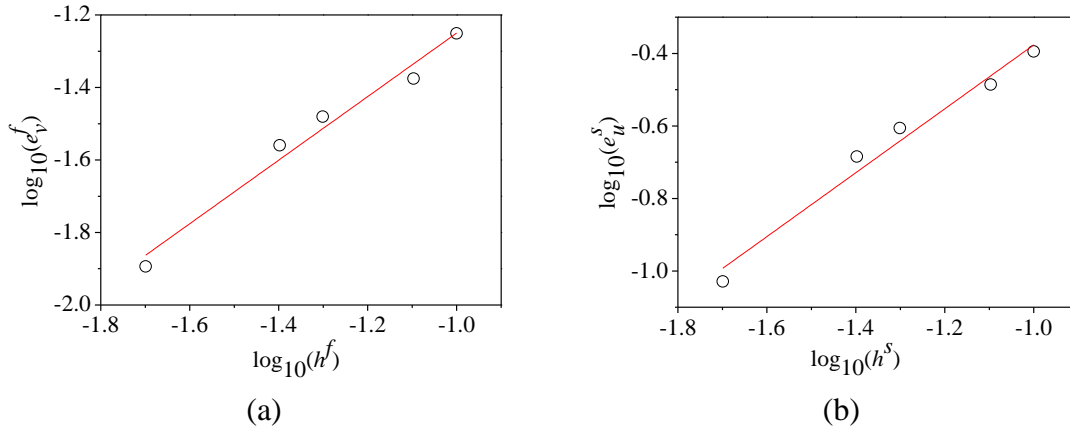


**Figure 3 The convergence analysis for the fluid domain (a) the fluid velocity (b) the solid displacement**

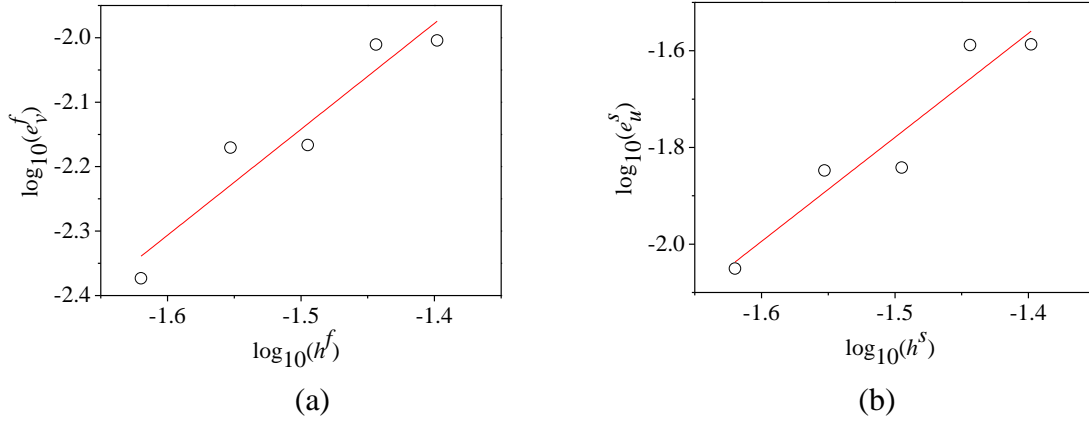


**Figure 4** The convergence analysis for the solid (a) the fluid velocity (b) the solid displacement

*A elastic beam in a fluid tunnel*

Here, a steady problem is considered about a flexible beam fixed in the fluid tunnel which was simulated previously using IS-FEM [15]. The viscous fluid flows across the beam and leads to a large deformation because of the fluid force. The beam will come to a steady state after some time when the elastic force balances with the fluid force. As illustrated in Figure 5, The length and height of the fluid field is  $L = 4$  cm and  $H = 1$  cm. The distance between the fixed beam and the left edge of the fluid tunnel is  $L/4$ . The thickness of the beam is  $a = 0.04$  cm and the height is  $b = 0.8$  cm. Gravity is neglected for this problem. The bottom of the fluid domain satisfies the nonslip boundary condition. And the top satisfies a symmetric condition using  $v_2^f = 0$ .

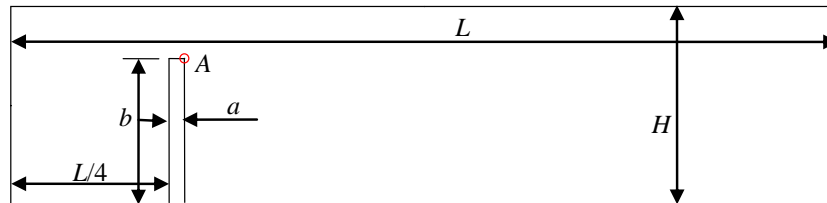


**Figure 5** Calculation model of beam in a fluid tunnel

We use  $800 \times 200$  uniform grids for fluid domain and irregular triangle elements with 409 nodes for the flexible beam. And Figure 6 have shown the result of velocity contour at the time  $t = 1s, 3s, 6s$ . A high velocity field arises on the upper of the beam because of the oscillation of the tip end and a low velocity field has been also formed behind the beam due to the barrier effect. And the fluid flow enforces the beam to bend along the fluid tunnel. The fluid force balances the elastic force gradually which brings out a stable state for the FSI system.

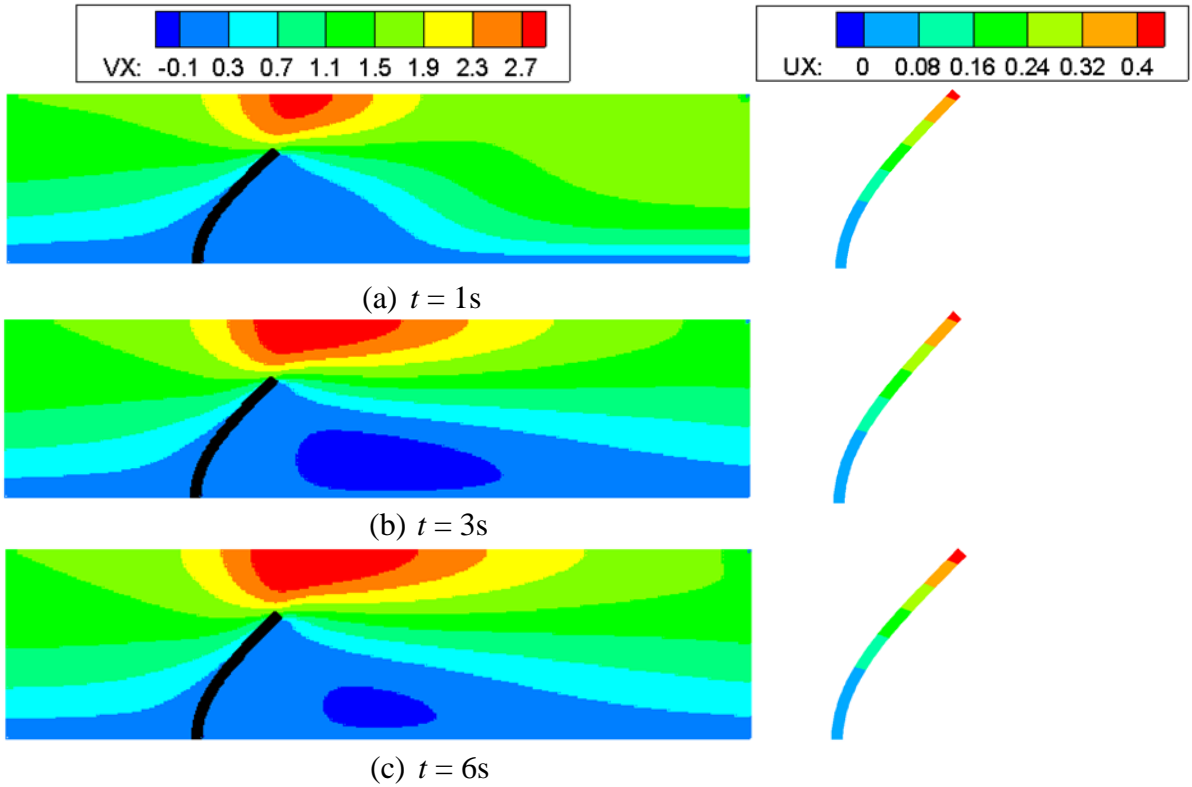


**Figure 6 Velocity contour and configuration of beam at different time**

(a)  $t=1s$  (b)  $t=3s$  (c)  $t= 6s$

The horizontal displacement of the tip in the beam has also been investigated in comparison with the result of reference solution, which can be found in Figure 7(a). The displacement amplitude in the balance state keeps consistent with the reported solution. Furthermore, we set a group of meshes to calculate the displacement errors to verify the advantages of S-PIM with FEM. The mesh sizes of solid domain are set as  $h^s=1/50$ ,  $1/75$ ,  $1/100$ , and  $1/125$  with the same fluid grid of  $h^f=1/100$ , and the reference solution is set  $h^s=1/200$  and  $h^f=1/100$  using FEM for solid solver. Figure 7(b) has shown the comparison result which validates the advantage of S-PIM for the solution of elastic problem.

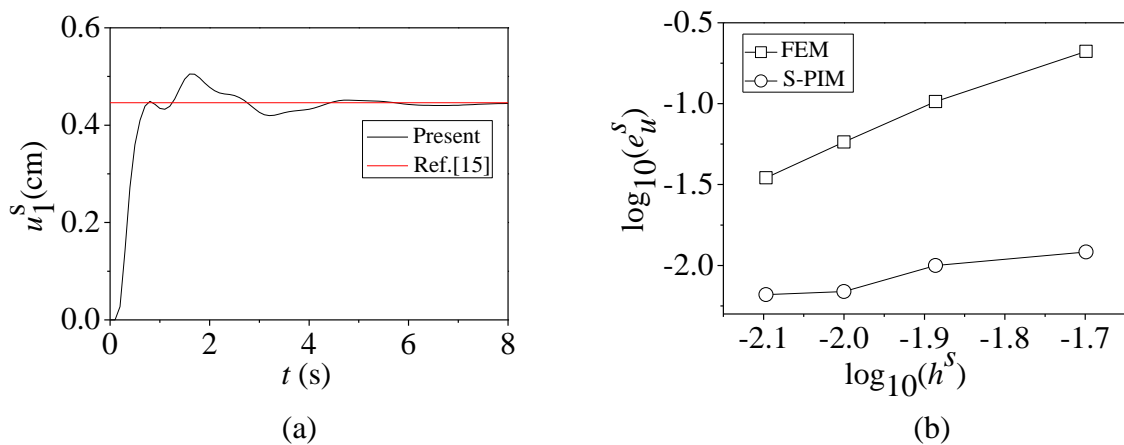


**Figure 7 (a) The curve of horizontal displacement in comparison with IS-FEM [15]**

**(b) The comparison of displacement errors in S-PIM and FEM**

Then the stress analysis of beam using S-PIM has been given in the Figure 8. And from the

figure, the beam encounters a primary tension-compression stress in y direction at the fixed bottom end and the fluid force leads to an obvious shear force around the middle of the beam.

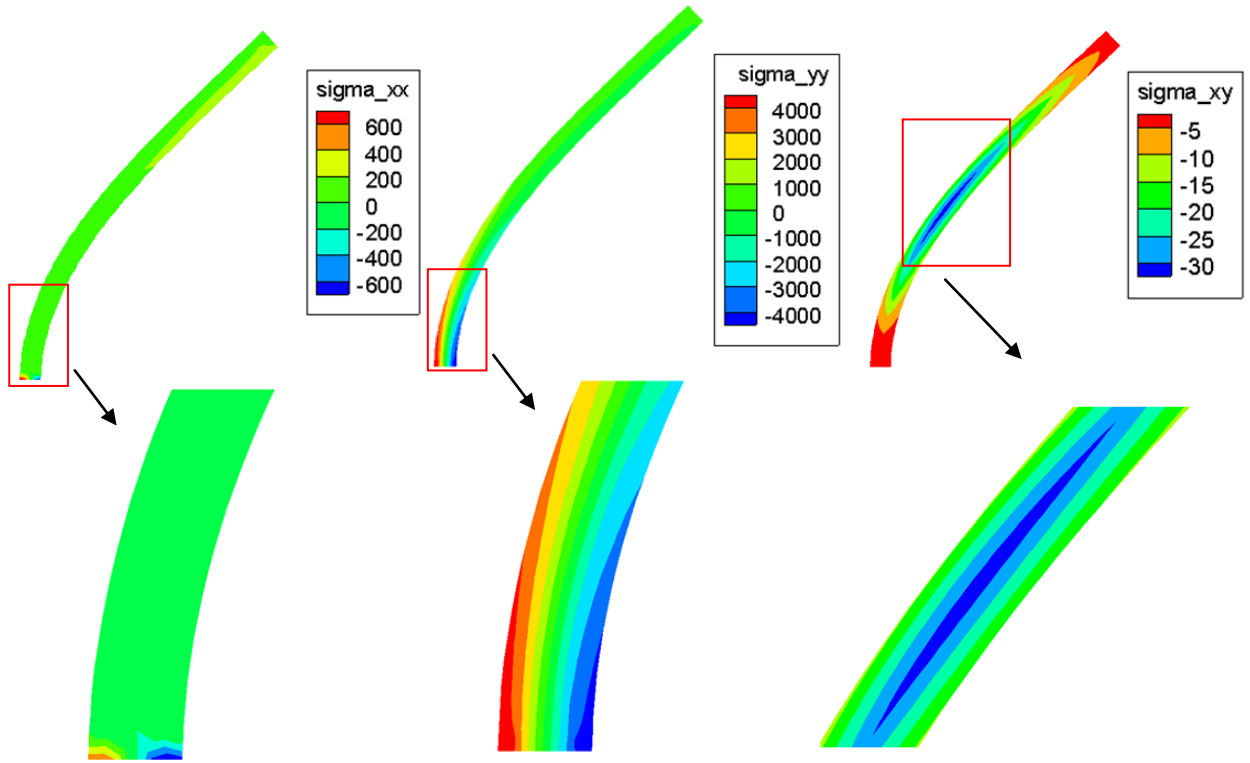


**Figure 8 The stress contour at the steady state**

#### *Flow passing a cylinder with a flexible flag*

A benchmark FSI problem of a cylinder with a flexible flag in the downstream side is analyzed to verify the reliability of IB-LBM with S-PIM. Here we consider the non-steady FSI case discussed by Turek and Hron [18]. As illustrated in Figure 9, the fluid domain is set as  $L = 2.5$  m and  $H = 0.41$  m, with a fixed circle of diameter  $d = 0.1$  m and centered at  $C = (0.2, 0.2)$  m. The elastic bar was attached at the right edge of the circle with the length  $l = 0.35$  m and height  $h = 0.02$  m. The fluid properties are given as  $\rho^f = 1.0 \times 10^3$  kg/m<sup>3</sup>,  $\mu^f = 1$  kg/(m·s) which means flow with a Reynolds number of  $Re = 100$ . The solid materials are modeled by Saint Venant-Kirchhoff with the density  $\rho^s = 10 \times 10^3$  kg/m<sup>3</sup>, Poisson's ratio  $\nu^s = 0.4$  and Young's modulus  $E^s = 0.5 \times 10^6$  kg/(m·s<sup>2</sup>). The boundary conditions are such that there is no slip over the top and bottom of the fluid channel together with the surface of the solid. At the outlet the pressure is set to be zero, and the input velocity  $v_x(t)$  has the following distribution:

$$v_x(t) = \begin{cases} \bar{v} \frac{1 - \cos(\pi t / 2)}{2} & t < 2.0 \\ \bar{v} & t \geq 2.0 \end{cases} \quad (21)$$

where  $\bar{v} = 1.5 \bar{U} y (H - y) / (H / 2)^2$ .

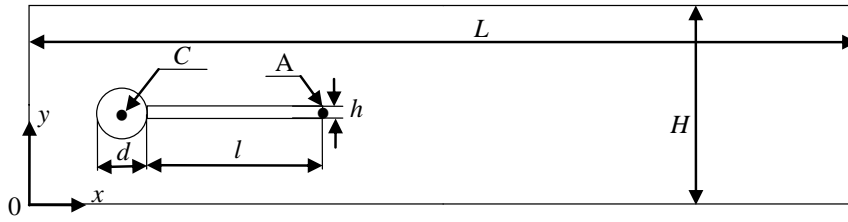


**Figure 9 Problem setting of fluid flow past a cylinder with a flag**

The fluid domain is discretized by  $1000 \times 164$  uniform grids. And Figure 10 shows the velocity contour at the time  $t=10$  s and  $t=13$  s. The fluid force enforces the flexible to swing and the vortex sheds along with flag as time varies.

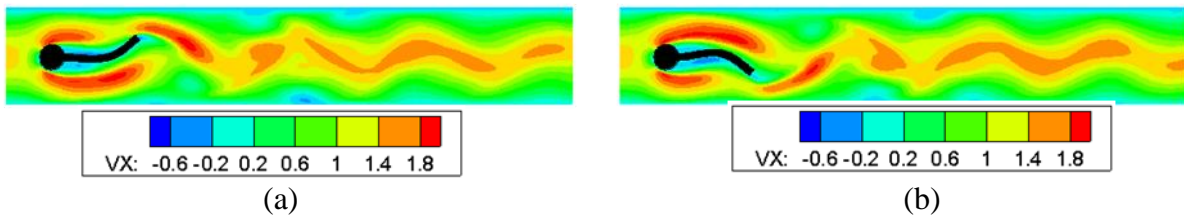
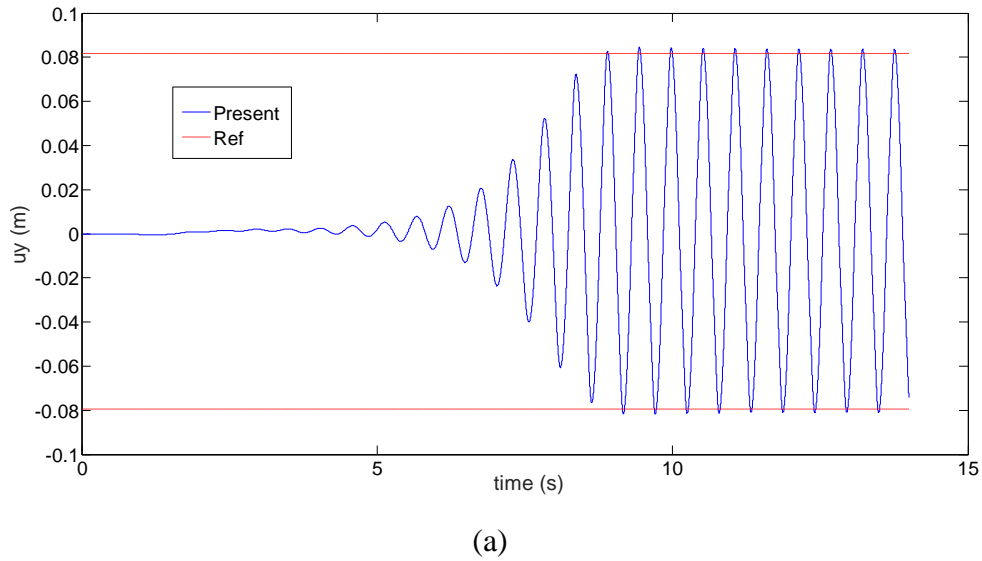
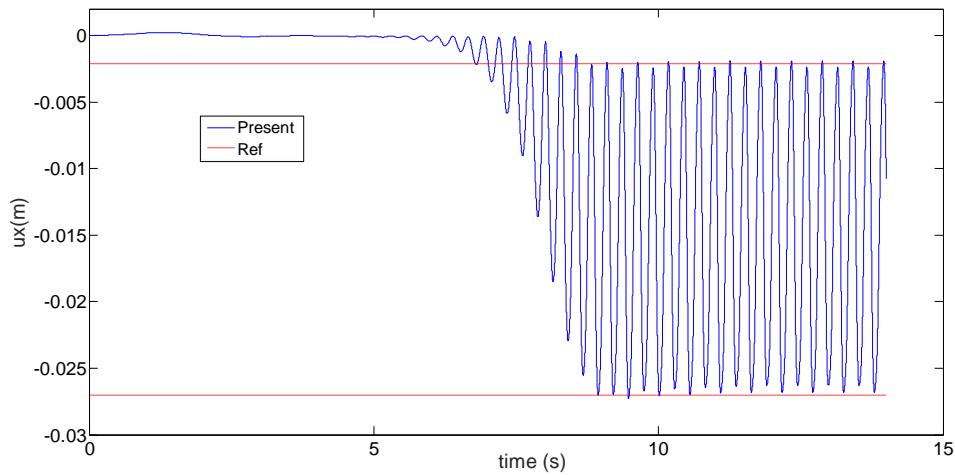


**Figure 10 Fluid velocity contours (a)  $t=10$ s (b)  $t=13$ s**

Figure 11 shows the displacement curve of the tail end in comparison with the reference result by vertical displacement  $u_y$  and horizontal displacement  $u_x$ , respectively. And from it, we can see a periodical vibration can be obtained after some time.



**(a)**



(b)

**Figure 11 The history of displacement at point A (a) vertical displacement  $u_y$   
(b) horizontal displacement  $u_x$**

## Conclusion

In this paper, we coupled IB-IBM with S-PIM to solve fluid-structure interaction problems with large deformable solids. Following conclusions can be obtained from the numerical examples:

- 1) The proposed method employs the framework of immersed boundary method which makes the method possess the advantages of avoiding re-meshing operation for moving interface.
- 2) The simple and efficient lattice Boltzmann method is used for incompressible viscous fluid flow with explicit evolution algorithm and avoids the solution of pressure Poisson equation.
- 3) The smoothed point interpolation method (S-PIM) is employed as solid solver which can soften the model stiffness and establish real constitutive equation for nonlinear analysis.
- 4) The better result can be obtained by S-PIM coupling with IB-LBM in comparison with coupled FEM for solid analysis.

## Acknowledgements:

The authors wish to thank the support of the National Natural Science Foundation of China (No. 51579042), the Key Program of National Natural Science Foundation of China (No. 51639003), the Recruitment program of Global Young Experts (NO. D1007001) and the Fundamental Research Funds for the Central Universities (DUT16ZD218).

## References

- [1] Peskin, C. (1977) Numerical analysis of blood flow in the heart. *Journal of Computational Physics* 25, 220–252.
- [2] Hughes, T.J.R., Franca, L.P. and Balestra, M. (1986) A new finite element formulation for computational fluid dynamics: V. Circumventing the babuška-brezzi condition: a stable Petrov-Galerkin formulation of the stokes problem accommodating equal-order interpolations. *Computer Methods in Applied Mechanics and Engineering* 59, 85-99.
- [3] Zienkiewicz, O.C., Nithiarasu, P., Codina, R., Vázquez, M. and Ortiz, P. (1999) The characteristic - based - split procedure: an efficient and accurate algorithm for fluid problems. *International Journal for Numerical*

*Methods in Fluids* 31, 359-392.

- [4] Feng, Z.G. and Michaelides, E.E. (2004) The immersed boundary-lattice Boltzmann method for solving fluid-particles interaction problems. *Journal of Computational Physics* 195, 602-628.
- [5] Feng, Z.G. and Michaelides, E.E. (2005) Proteus: a direct forcing method in the simulations of particulate flows. *Journal of Computational Physics* 202, 20-51.
- [6] Niu, X.D., Shu, C., Chew, Y.T. and Peng, Y. (2006) A momentum exchange-based immersed boundary-lattice Boltzmann method for simulating incompressible viscous flows. *Physics Letters A* 354, 173-182.
- [7] Dupuis, A., Chatelain, P. and Koumoutsakos, P. (2008) An immersed boundary-lattice-Boltzmann method for the simulation of the flow past an impulsively started cylinder. *Journal of Computational Physics* 227, 4486-4498.
- [8] Liu, G.R. and Nguyen-Thoi, T. *Smoothed Finite Element Methods*. 2010, Boca Raton: CRC Press
- [9] Liu, G.R., Nguyen-Thoi, T. and Lam, K.Y. (2009) An edge-based smoothed finite element method (ES-FEM) for static, free and forced vibration analyses of solids. *J Sound Vib* 320, 1100-1130.
- [10] Liu, G.R., Nguyen-Thoi, T. and Lam, K.Y. (2009) Edge-based smoothed point interpolation methods. *Int J Comp Meth-Sing* 5, 621-646.
- [11] Liu, G.R. and Zhang, G.Y. *Smoothed Point Interpolation Methods: G Space and Weakened Weak Forms*. 2013, Singapore: World Scientific Press.
- [12] Guo, Z., Zheng, C. and Shi, B. (2002) Discrete lattice effects on the forcing term in the lattice Boltzmann method. *Physical review. E, Statistical, nonlinear, and soft matter physics* 65, 046308.
- [13] Qian, Y.H. (1992) Lattice bkg models for navier-stokes equation. *EPL (Europhysics Letters)* 17, 479-484.
- [14] Kang, S.K. and Hassan, Y.A. (2011) A comparative study of direct-forcing immersed boundary-lattice Boltzmann methods for stationary complex boundaries. *International Journal for Numerical Methods in Fluids* 66, 1132-1158.
- [15] Zhang, Z.Q., Liu, G.R. and Khoo, B.C. (2012) Immersed smoothed finite element method for two dimensional fluid-structure interaction problems. *Int J Numer Meth Eng* 90, 1292-1320.
- [16] Dunne, T. (2006) An Eulerian approach to fluid-structure interaction and goal - oriented mesh adaptation. *International Journal for Numerical Methods in Fluids* 51, 1017-1039.
- [17] Wang, X. and Zhang, L.T. (2010) Interpolation functions in the immersed boundary and finite element methods. *Comput Mech* 45, 321-334.
- [18] Turek S and Hron J, Proposal for Numerical Benchmarking of Fluid-Structure Interaction Between an Elastic Object and Laminar Incompressible Flow, in *Fluid-structure interaction (Lecture Notes in Computational Science and Engineering)*, S. e. Bungartz H-J, Editor. 2006, Springer: Berlin, Heidelberg. p. 371-385.2006